NANO LETTERS

Letter

pubs.acs.org/NanoLett

Chemical Vapor Deposition-Derived Graphene with Electrical Performance of Exfoliated Graphene

Nicholas Petrone,[†] Cory R. Dean,[†,‡] Inanc Meric,[‡] Arend M. van der Zande,[†] Pinshane Y. Huang,[§] Lei Wang,[†] David Muller,[§,∥] Kenneth L. Shepard,[‡] and James Hone*[,†]

[†]Department of Mechanical Engineering and [‡]Department of Electrical Engineering, Columbia University, New York, New York 10027, United States

[§]School of Applied and Engineering Physics and [∥]Kavli Institute at Cornell University, Cornell University, Ithaca, New York 14853, United States

Supporting Information

ABSTRACT: While chemical vapor deposition (CVD) promises a scalable method to produce large-area graphene, CVD-grown graphene has heretofore exhibited inferior electronic properties in comparison with exfoliated samples. Here we test the electrical transport properties of CVD-grown graphene in which two important sources of disorder, namely grain boundaries and processing-induced contamination, are substantially reduced. We grow CVD graphene with grain sizes up to 250 μm to abate grain boundaries, and we transfer graphene utilizing a novel, dry-transfer method to minimize chemical contamination. We fabricate devices on both silicon dioxide and hexagonal boron nitride (h-BN) dielectrics to probe the effects of substrate-induced disorder. On both substrate types, the large-grain CVD graphene samples are comparable in quality to the best reported exfoliated samples, as determined by low-temperature electrical transport and magnetotransport measurements. Small-grain samples exhibit much greater variation in quality and inferior performance by multiple measures, even in samples exhibiting high field-effect mobility. These results confirm the possibility of achieving high-performance graphene devices based on a scalable synthesis process.

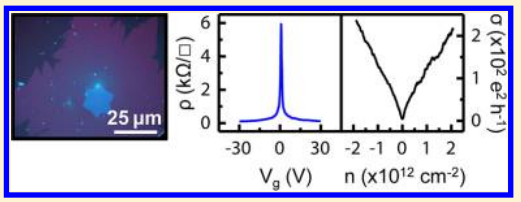

KEYWORDS: *Graphene, CVD, boron nitride, grain, mobility*

Chemical vapor deposition (CVD) offers a promising method to produce large-area films of graphene, crucial for the commercial realization of graphene-based applications. However, the electronic performance of CVD-grown graphene has remained problematic. Compared to exfoliated graphene, CVD graphene exhibits lower mobility, greater impurity doping, and higher asymmetry between electron and hole conduction.[1−7] These differences are indicative of disorder and scattering processes that are not present in exfoliated samples. Lattice defects and grain boundaries resulting from the growth process[1,8] as well as structural defects and chemical contamination introduced during transfer[1−3,8−10] have all been identified as sources of disorder in CVD-grown graphene devices. While recent work has shown progress in increasing grain size[4,7] and reducing transfer-related contamination,[11,12] no work has yet demonstrated that CVD graphene can achieve repeatable performance comparable to that of exfoliated graphene.

In this letter, we present a detailed study of the electrical transport behavior of CVD graphene in which both grain boundary scattering is eliminated and transfer-induced contamination is minimized. To eliminate grain boundaries within fabricated devices, we synthesize CVD graphene with large grain sizes, up to 250 μm in dimension.[2−4] To reduce contamination during processing, we employ a novel dry transfer technique which greatly reduces the extrinsic doping of CVD graphene devices. Samples are fabricated both on SiO_2 and on hexagonal boron nitride (h-BN), a dielectric which minimizes substrate-induced scattering and permits for the most precise assessment of the intrinsic performance of graphene.[13] Device performance is characterized by low-temperature electrical transport and magnetotransport measurements. These measurements demonstrate, for the first time, that chemically synthesized graphene can reproducibly achieve electrical performance comparable to that of high-quality exfoliated graphene.

We grow single-layer graphene with crystallographic domains up to several hundred micrometers in dimension on copper foil using a recently reported low-pressure, encapsulated CVD growth method,[4] (see Supporting Information for growth details). Figure 1a shows an optical micrograph of graphene grown by CVD and subsequently transferred onto SiO_2, demonstrating that the encapsulated growth technique utilized in this work results in discrete, star-shaped patches of graphene with dimensions controllable between 20 and 250 μm by varying the CVD growth time. In order to determine the graphene's grain structure, we use dark-field transmission

Received: December 19, 2011
Revised: May 8, 2012

   dx.doi.org/10.1021/nl204481s | *Nano Lett.* XXXX, XXX, XXX−XXX

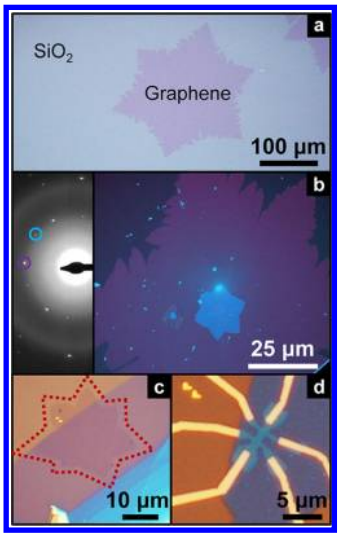

Figure 1. (a) Optical micrograph of large-grain CVD graphene transferred onto SiO_2. (b) False-colored DF-TEM image of large-grain CVD graphene. A small, second layer (blue) is apparent in the center of the large graphene crystal (purple). Inset in (b) is the electron diffraction pattern corresponding to the area of the DF-TEM image; the colored circles outline spots corresponding to different grain orientations, indicating that the two graphene layers apparent in (b) are each single crystalline and rotationally misaligned from one another. (c) Large-grain CVD graphene crystal (outlined with a dashed line for clarity) transferred onto a h-BN flake using the dry transfer method. (d) Completed Hall bar device fabricated on a h-BN substrate.

electron microscopy (DF-TEM).[1] Figure 1b shows a false-colored DF-TEM map of the CVD graphene, with each color in the figure corresponding to a unique crystallographic orientation. The color map in Figure 1b indicates that the large, star-shaped graphene patches are largely single crystalline, containing no grain boundaries. Occasionally, we observe a small, second layer in the center of a large crystal, as is apparent in Figure 1b. The two sets of six-fold symmetric spots present in the corresponding electron diffraction pattern (Figure 1b, inset) indicate that each layer is a single domain, with the layers rotationally misaligned from one another. During fabrication of electronic devices, we avoid these small double-layer areas and study the transport properties only of monolayer regions. For comparison, we also synthesize graphene by more conventional CVD methods,[1−3] which yield continuous films of polycrystalline graphene with grain sizes typically less than 5 μm in dimension (see Supporting Information for details on growth procedure and grain-structure analysis). Below we refer to these two sample types as large- and small-grain CVD graphene, respectively.

In typical processing methods used to fabricate graphene devices from CVD grown material,[2,9,14] the graphene film is first released from the growth substrate using a chemical etch and then subsequently rinsed in baths of deionized (DI) water. The film is then transferred onto a process substrate, resulting in the drying of a layer of DI water between the CVD graphene and underlying substrate. The use of this wet transfer process typically results in graphene films with high concentrations of p-type dopants ($\geq 4 \times 10^{12}$ cm^{-2}) and low electronic mobility (500−10 000 cm^2 V^{-1} s^{-1}).[1,2,5−7,15] While procedures that circumvent the wet transfer step have been reported to reduce the introduction of disorder from the trapping of impurities present in the DI water at the graphene−dielectric interface,[11,12] so far none has yielded transferred CVD graphene films with demonstrated improvement in mobility.

In this study, we employ an alternative dry transfer procedure to minimize the introduction of ionic impurities at the graphene−dielectric interface. After CVD growth, a layer of PMMA is spin coated onto the graphene surface. Next, the opposite side of the copper foil is adhered over a small (~1 cm) window cut in the center of a piece of polyimide tape (3M #5413). The exposed copper is then etched in ammonium persulfate (Transene APS-100), yielding a thin PMMA/graphene membrane suspended across the window. The sample is subsequently rinsed in isopropanol and blown dry with nitrogen to prevent liquid from drying on the graphene's surface. Finally, the graphene is transferred under dry conditions onto the target substrate. An additional advantage of this technique is that it allows for aligned transfer of the graphene. Figure 1c shows an optical micrograph of a star-shaped graphene crystal transferred onto a preselected h-BN flake that was first mechanically exfoliated onto a silicon substrate with 285 nm thermally grown SiO_2[13] (see Supporting Information for further details on the transfer method).

Following transfer, the graphene samples were patterned into Hall bars with nominal channel widths of 1 μm and lengths of 1.5 μm, as measured from the center of the voltage probes, using electron beam lithography and oxygen plasma etching. A second lithography step was then used to pattern electrodes onto the devices. Figure 1d shows an optical micrograph of a typical CVD graphene device fabricated on a h-BN flake. Prior to measurement, samples were annealed in forming gas at 345 °C to remove resist residue. Atomic force microscopy (AFM) was used to verify device dimensions and confirm the absence of contamination or structural defects in the graphene (see Supporting Information). Sample resistivity was measured using four-terminal geometry and standard lock-in techniques at 1.6 K; measurements were taken in both liquid ^{4}He cryostats with sample in He vapor and a continuous flow cryostat with sample in vacuum. The conductive silicon wafer was used as the back gate for all devices; the gate capacitance, C_g, was determined directly from Hall effect measurements.

Figure 2a shows the resistivity as a function of gate voltage, V_g, for a large-grain device on h-BN. Several features immediately distinguish the transport characteristics of this device from those of previously reported CVD-grown graphene.[1,5−7,9,16] The sample exhibits a narrow resistivity peak (full width at half-maximum ~1.5 V), with the charge neutrality point (CNP) near $V_g = 0$ (V_0 ~0.8 V). In addition, the sample shows low resistivity (~120 Ω/□) at high carrier density. These features indicate a lack of disorder and static doping from charged impurities.[17−20] Figure 2b shows the conductivity as a function of carrier density, n (given by $n = C_g(V_g - V_0)/e$). The conductivity is remarkably linear in n, with identical slopes for both positive and negative carriers. Figure 2c shows the density-dependent field-effect mobility, μ_{FE}, computed directly from the conductivity data by $\mu_{FE} = \sigma/ne$.[21,22] Remarkably, μ_{FE} ranges between ~30 000 cm^2 V^{-1} s^{-1} at high density to greater than 50 000 cm^2 V^{-1} s^{-1} at densities less than 5×10^{11} cm^{-2}.

In order to more completely characterize the electronic properties of our device and to distinguish among the effects of various sources of disorder, we fit the conductivity data with a commonly employed self-consistent diffusive transport model,[17] $\sigma^{-1} = (ne\mu_c + \sigma_o)^{-1} + \rho_s$. In this model, μ_c is the

dx.doi.org/10.1021/nl204481s | Nano Lett. XXXX, XXX, XXX−XXX

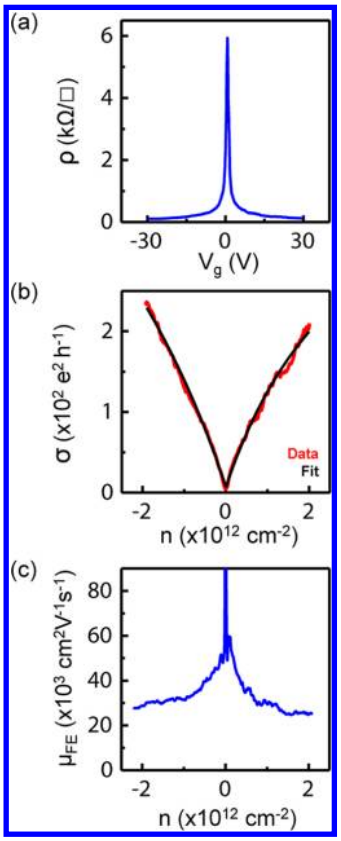

Figure 2. Electronic transport data for a large-grain CVD graphene device fabricated on a h-BN dielectric. Plot of (a) resistivity as a function of gate voltage and (b) conductivity as a function of carrier density. Conductivity data is plotted in red, with a fit to the data by a Boltzmann model for diffusive transport plotted in black. (c) Plot of field-effect mobility as a function of carrier density. Electronic transport data taken at 1.6 K.

density-independent mobility attributed to long-range, charged impurity Coulomb scattering; ρ_s is a constant contribution to resistivity from short-range scattering; and σ_o is the residual conductivity at the Dirac point. For uniformity of comparison, we always present values of μ_{FE} and μ_c corresponding to positive charge carriers. As shown in Figure 2b, this model reproduces the conductivity data well. The extracted density-independent mobility for this device is $\mu_c = 45\,000$ cm^2 V^{-1} s^{-1}. This is the highest value of μ_c for a CVD-grown graphene device reported to date: nearly twice that of the best value reported on SiO_2[7] and 20% larger than the only reported measurement of CVD graphene on h-BN, which was fabricated from small-grain graphene.[16] More importantly, this mobility is comparable to values observed for exfoliated graphene on h-BN.[13]

We can additionally characterize the disorder present in our large-grain devices by the full width at half-maximum of the resistivity peak with respect to carrier density, ΔW_{CNP}, which places an upper bound on the carrier density fluctuations owing to disorder,[18,23] and by the observed position of the CNP, which provides an indication of the intrinsic doping levels.[19,20] For the sample shown in Figure 2, $V_0 \sim 0.8$ V and $\Delta W_{CNP} \sim 8 \times 10^{-10}$ cm^{-2}; both measures confirm that our large-grain CVD graphene samples on h-BN possess low concentrations of dopants and charged impurities,[17−20] and they are consistent with typical values reported for exfoliated graphene on h-BN.[13]

Figure 2b reveals that large-grain CVD-derived graphene can actually exceed the performance of exfoliated graphene by one measure: namely, the conductivity curve is remarkably linear in comparison to those reported for exfoliated devices of similar mobility, leading to a correspondingly small value of ρ_s.[13,19] In the simplest interpretation, this difference implies that large-grain CVD graphene possesses fewer sources of short-range disorder than exfoliated graphene does. We note, however, that the origin of such short-range scattering in exfoliated devices remains unclear. For example, competing models attribute the sublinear shape of the conductivity curve typically observed in samples exhibiting similarly high mobility to different mechanisms, such as resonant scattering[24] and spatial correlations in charged impurities.[25] A more complete analysis of the structural differences between exfoliated and large-grain CVD graphene may help discriminate among these possible scattering mechanisms. However, regardless of the scattering mechanism, these results suggest that CVD graphene may achieve high-density conductivity exceeding that of exfoliated graphene, which would have important implications for applications such as transparent conducting films.

Magnetotransport measurements provide a further demonstration of sample quality. Figure 3a shows a Landau fan

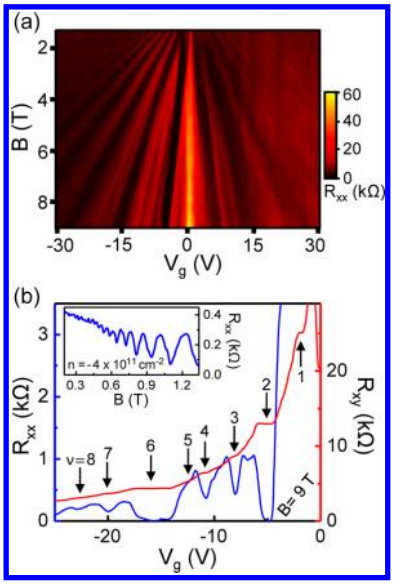

Figure 3. (a) Landau fan diagram of longitudinal resistance, R_{xx}, as a function of gate voltage, V_g, and magnetic field, B. (b) Corresponding plot of longitudinal resistance, R_{xx}, measured on left axis and Hall resistance, R_{xy}, measured on right axis as a function of V_g taken at a fixed magnetic field of 9 T. Inset of (b) plots R_{xx} as a function of B at a fixed carrier density of -4×10^{11} cm^{-2}. Magnetotransport data taken at 1.6 K.

diagram for the device depicted in Figure 2, with R_{xx} plotted as a function of magnetic field, B, and gate voltage, V_g. Quantum Hall effect (QHE) minima, corresponding to filling factor, ν, appear as stripes fanning out from $B = 0$ T. Fully quantized QHE plateaus appear at magnetic fields below 2 T, and symmetry breaking of the four-fold Landau level degeneracy is seen below 5 T. Figure 3b shows clear signatures of all quantum Hall states at filling fractions 1−8 at $B = 9$ T; the onset of Shubnikov−de Haas oscillations for this sample is observed at fields below 400 mT, as shown in the figure's inset. Such characteristics of magnetotransport have previously only been

dx.doi.org/10.1021/nl204481s | Nano Lett. XXXX, XXX, XXX−XXX

reported for exfoliated samples with similar mobilities (see, for example, ref 13).

In order to assess the repeatability of the large-grain device performance, we measured and compared the transport characteristics of multiple large-grain CVD devices fabricated on both SiO_2 and h-BN. In addition, to determine how the dry transfer technique affects the performance of small-grain CVD graphene, we fabricated small-grain devices on SiO_2 and h-BN. Figure 4 shows representative resistivity data for three devices

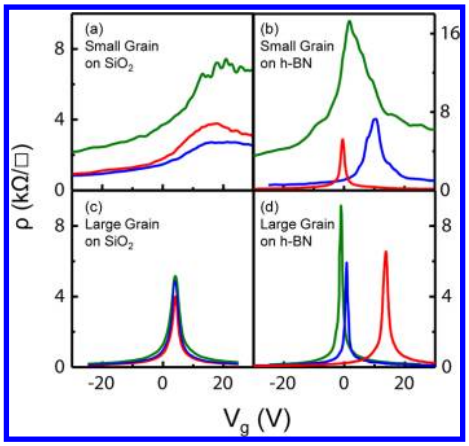

Figure 4. Resistivity data plotted as a function of gate voltage for multiple devices of each combination of CVD graphene grain size and dielectric material. Data are presented for three devices of each of the following configurations: (a) small-grain graphene on SiO_2, (b) small-grain graphene on h-BN, (c) large-grain graphene on SiO_2, and (d) large-grain graphene on h-BN. Data taken at 1.6 K.

fabricated from each grain size and substrate combination. The data were analyzed as above to yield quantitative measures of sample quality, summarized in Table S1, Supporting Information.

We first note that every sample, regardless of substrate, shows a dopant concentration between 1.2×10^{10} and 1.6×10^{12} cm^{-2}, lower than values previously reported for CVD graphene processed by either wet transfer[5,16] or dry transfer[11,12] methods. We take this as evidence that the transfer procedure employed in this study successfully reduces the introduction of charged dopants compared to other techniques. Moreover, a majority of devices fabricated on h-BN show doping levels below 6×10^{10} cm^{-2}, demonstrating that the procedure is capable of achieving extremely low levels of charged impurity contamination.

All of the large-grain samples measured show uniformly outstanding performance that is indistinguishable from that of exfoliated graphene by all of the measures discussed above. In particular, the resistivity curves in Figure 4c,d show narrow, symmetric Dirac peaks and low resistivity at high gate voltage. Large-grain graphene on SiO_2 (Figure 4c) displays μ_c ranging between 17 000 and 25 000 cm^2 V^{-1} s^{-1}, higher than the best reported values for CVD graphene[7] and equivalent to the best reported values for exfoliated graphene[21,22] on SiO_2. Likewise, large-grain graphene on h-BN (Figure 4d) shows μ_c ranging between 27 000 and 45 000 cm^2 V^{-1} s^{-1}. For comparison, in Figure S5, Supporting Information, we plot the distribution of μ_c values extracted for multiple samples of exfoliated graphene on h-BN, produced in our laboratory in the context of other studies.[13] The three large-grain CVD samples studied in this work lie well within this distribution. The measured Dirac peak widths on both substrate types lie below 3×10^{11} cm^{-2}, indicating low disorder. Finally, large-grain samples all show low values of ρ_s, below those typically seen for exfoliated graphene. All of these metrics demonstrate that large-grain CVD graphene is capable of achieving repeatable electronic properties equivalent to those of exfoliated graphene, essential to device applications. Furthermore, the systematic shift toward higher mobility in devices on h-BN also indicates that the dominant scattering mechanism for SiO_2 supported large-grain CVD graphene devices is disorder originating from the substrate, rather than from the crystallographic structure or from process-related contamination.

Figure 4 further demonstrates that the average performance of small-grain graphene is inferior to that of large-grain graphene, and small-grain samples exhibit much higher sample-to-sample variability in electronic characteristics. On SiO_2, small-grain samples all show broad resistivity peaks with a high degree of asymmetry between positive and negative charge carriers. For these samples, μ_c ranges between 1,200 and 2,300 cm^2 V^{-1} s^{-1}, comparable to values reported previously for graphene grown with similar grain structure.[1−3,5,6] Small-grain graphene on h-BN shows extreme variability: some samples display broad, asymmetric resistivity peaks similar to those seen for small-grain samples on SiO_2, while others show very narrow peaks similar to those seen for large-grain samples on h-BN. In fact, the best such sample has μ_c = 65 500 cm^2 V^{-1} s^{-1}, nominally superior to all large-grain samples measured. This result is consistent with a previous report of a high-mobility CVD graphene device on h-BN.[16] However, it is important to note that mobility is not a complete measure of sample quality. Both high-mobility small-grain devices measured here, as well as the previously reported device, show highly asymmetric transport characteristics. Such asymmetry can be a signature of resonant scattering, which can lead to anomalously high field-effect mobility due to the energy dependence of the mean free path.[24] In addition, at high density, small-grain samples show comparatively lower μ_{FE} and higher ρ_s. (See Supporting Information for further information on electronic transport data for small-grain samples.)

It is interesting to speculate as to why some small-grain samples on h-BN show very high performance. The simplest explanation is that these samples are fabricated within a single graphene grain. However, this explanation is unable to account for other features, such as electron−hole asymmetry, also observed in these samples. Moreover, in such a picture, some of the small-grain samples on SiO_2 would be expected to show performance close to that of large-grain samples on SiO_2 (e.g., $\mu_c \sim 20\,000$ cm^2 V^{-1} s^{-1}). However, none of our samples, nor any reported in the literature,[1−7] demonstrates comparable electronic characteristics. Thus electronic transport in small-grain CVD graphene seems to be more complicated, with interactions between the grain structure, processing technique, and substrate composition that are still not well understood. This not only motivates further study but also highlights the advantages of large-grain in comparison to small-grain graphene.

This work represents the first demonstration that CVD graphene can achieve repeatable electronic performance comparable to that of exfoliated graphene, by multiple measures. As such, it sets the stage for utilizing CVD graphene both for fundamental studies and for high performance graphene-based technologies. These results further motivate the growing need for complementary technological advance-

dx.doi.org/10.1021/nl204481s | Nano Lett. XXXX, XXX, XXX−XXX

ments, such as scalable growth of high-quality dielectrics, essential to the ultimate performance of large-area graphene devices.

■ ASSOCIATED CONTENT

Supporting Information

Further details are provided related to graphene growth procedures, characterization of the crystallographic structure of CVD graphene, dry transfer method, and device fabrication. Additional data from Hall bar devices are presented for CVD graphene samples, including AFM data, resistivity and field-effect mobility data for the highest mobility device measured, and a tabulation of derived transport parameters. Mobility values for exfoliated samples fabricated on h-BN are also presented. This material is available free of charge via the Internet at http://pubs.acs.org.

■ AUTHOR INFORMATION

Corresponding Author

*E-mail: jh2228@columbia.edu.

Notes

The authors declare no competing financial interest.

■ ACKNOWLEDGMENTS

We thank Prof. Philip Kim for helpful discussions and for providing access to facilities for magnetotransport measurements. We also thank Dr. Andrea Young for help with magnetotransport measurements and data analysis. N.P. thanks Prof. Changgu Lee, Prof. Keunsoo Kim, and Dr. Gwan Hyoung Lee for helpful discussions and Walker Kahn and Robert Stark for technical support. We gratefully acknowledge support by DARPA under contract FA8650-08-C-7838 through the CERA program and by the AFOSR MURI Program on new graphene materials technology, FA9550-09-1-0705. This work was partially funded by the U.S. Department of Energy EFRC program (grant DE-SC00001085). We also acknowledge support by the NSF through the Cornell Center for Materials Research (NSF DMR-1120296) and the National Science Foundation Graduate Research Fellowship under grant no. DGE-0707428 (for P.Y.H)

■ REFERENCES

(1) Huang, P. Y.; Ruiz-Vargas, C. S.; van der Zande, A. M.; Whitney, W. S.; Levendorf, M. P.; Kevek, J. W.; Garg, S.; Alden, J. S.; Hustedt, C. J.; Zhu, Y.; Park, J.; McEuen, P. L.; Muller, D. A. Grains and grain boundaries in single-layer graphene atomic patchwork quilts. *Nature* **2011**, *469* (7330), 389−392.

(2) Li, X. S.; Cai, W. W.; An, J. H.; Kim, S.; Nah, J.; Yang, D. X.; Piner, R.; Velamakanni, A.; Jung, I.; Tutuc, E.; Banerjee, S. K.; Colombo, L.; Ruoff, R. S. Large-Area Synthesis of High-Quality and Uniform Graphene Films on Copper Foils. *Science* **2009**, *324* (5932), 1312−1314.

(3) Bae, S.; Kim, H.; Lee, Y.; Xu, X. F.; Park, J. S.; Zheng, Y.; Balakrishnan, J.; Lei, T.; Kim, H. R.; Song, Y. I.; Kim, Y. J.; Kim, K. S.; Ozyilmaz, B.; Ahn, J. H.; Hong, B. H.; Iijima, S. Roll-to-roll production of 30-in. graphene films for transparent electrodes. *Nat. Nanotechnol.* **2010**, *5* (8), 574−578.

(4) Li, X. S.; Magnuson, C. W.; Venugopal, A.; Tromp, R. M.; Hannon, J. B.; Vogel, E. M.; Colombo, L.; Ruoff, R. S. Large-Area Graphene Single Crystals Grown by Low-Pressure Chemical Vapor Deposition of Methane on Copper. *J. Am. Chem. Soc.* **2011**, *133* (9), 2816−2819.

(5) Cao, H. L.; Yu, Q. K.; Jauregui, L. A.; Tian, J.; Wu, W.; Liu, Z.; Jalilian, R.; Benjamin, D. K.; Jiang, Z.; Bao, J.; Pei, S. S.; Chen, Y. P. Electronic transport in chemical vapor deposited graphene synthesized on Cu: Quantum Hall effect and weak localization. *Appl. Phys. Lett.* **2010**, *96*, 25.

(6) Venugopal, A.; Chan, J.; Li, X. S.; Magnuson, C. W.; Kirk, W. P.; Colombo, L.; Ruoff, R. S.; Vogel, E. M. Effective mobility of single-layer graphene transistors as a function of channel dimensions. *J. Appl. Phys.* **2011**, *109*, 10.

(7) Li, X. S.; Magnuson, C. W.; Venugopal, A.; An, J. H.; Suk, J. W.; Han, B. Y.; Borysiak, M.; Cai, W. W.; Velamakanni, A.; Zhu, Y. W.; Fu, L. F.; Vogel, E. M.; Voelkl, E.; Colombo, L.; Ruoff, R. S. Graphene Films with Large Domain Size by a Two-Step Chemical Vapor Deposition Process. *Nano Lett.* **2010**, *10* (11), 4328−4334.

(8) An, J. H.; Voelkl, E.; Suk, J. W.; Li, X. S.; Magnuson, C. W.; Fu, L. F.; Tiemeijer, P.; Bischoff, M.; Freitag, B.; Popova, E.; Ruoff, R. S. Domain (Grain) Boundaries and Evidence of "Twinlike" Structures in Chemically Vapor Deposited Grown Graphene. *ACS Nano* **2011**, *5* (4), 2433−2439.

(9) Li, X. S.; Zhu, Y. W.; Cai, W. W.; Borysiak, M.; Han, B. Y.; Chen, D.; Piner, R. D.; Colombo, L.; Ruoff, R. S. Transfer of Large-Area Graphene Films for High-Performance Transparent Conductive Electrodes. *Nano Lett.* **2009**, *9* (12), 4359−4363.

(10) Levendorf, M. P.; Ruiz-Vargas, C. S.; Garg, S.; Park, J. Transfer-Free Batch Fabrication of Single Layer Graphene Transistors. *Nano Lett.* **2009**, *9* (12), 4479−4483.

(11) Suk, J. W.; Kitt, A.; Magnuson, C. W.; Hao, Y. F.; Ahmed, S.; An, J. H.; Swan, A. K.; Goldberg, B. B.; Ruoff, R. S. Transfer of CVD-Grown Monolayer Graphene onto Arbitrary Substrates. *ACS Nano* **2011**, *5* (9), 6916−6924.

(12) Lock, E. H.; Baraket, M.; Laskoski, M.; Mulvaney, S. P.; Lee, W. K.; Sheehan, P. E.; Hines, D. R.; Robinson, J. T.; Tosado, J.; Fuhrer, M. S.; Hernandez, S. C.; Walton, S. G. High-Quality Uniform Dry Transfer of Graphene to Polymers. *Nano Lett.* **2011**, *12* (1), 102−107.

(13) Dean, C. R.; Young, A. F.; Meric, I.; Lee, C.; Wang, L.; Sorgenfrei, S.; Watanabe, K.; Taniguchi, T.; Kim, P.; Shepard, K. L.; Hone, J. Boron nitride substrates for high-quality graphene electronics. *Nat. Nanotechnol.* **2010**, *5* (10), 722−726.

(14) Kim, K. S.; Zhao, Y.; Jang, H.; Lee, S. Y.; Kim, J. M.; Kim, K. S.; Ahn, J. H.; Kim, P.; Choi, J. Y.; Hong, B. H. Large-scale pattern growth of graphene films for stretchable transparent electrodes. *Nature* **2009**, *457* (7230), 706−710.

(15) Yu, Q. K.; Jauregui, L. A.; Wu, W.; Colby, R.; Tian, J. F.; Su, Z. H.; Cao, H. L.; Liu, Z. H.; Pandey, D.; Wei, D. G.; Chung, T. F.; Peng, P.; Guisinger, N. P.; Stach, E. A.; Bao, J. M.; Pei, S. S.; Chen, Y. P. Control and characterization of individual grains and grain boundaries in graphene grown by chemical vapour deposition. *Nat. Mater.* **2011**, *10* (6), 443−449.

(16) Gannett, W.; Regan, W.; Watanabe, K.; Taniguchi, T.; Crommie, M. F.; Zettl, A. Boron nitride substrates for high mobility chemical vapor deposited graphene. *Appl. Phys. Lett.* **2011**, *98*, 24.

(17) Hwang, E. H.; Adam, S.; Das Sarma, S. Carrier transport in two-dimensional graphene layers. *Phys. Rev. Lett.* **2007**, *98*, 18.

(18) Bolotin, K. I.; Sikes, K. J.; Jiang, Z.; Klima, M.; Fudenberg, G.; Hone, J.; Kim, P.; Stormer, H. L. Ultrahigh electron mobility in suspended graphene. *Solid State Commun.* **2008**, *146* (9−10), 351−355.

(19) Chen, J. H.; Jang, C.; Adam, S.; Fuhrer, M. S.; Williams, E. D.; Ishigami, M. Charged-impurity scattering in graphene. *Nat Phys* **2008**, *4* (5), 377−381.

(20) Tan, Y. W.; Zhang, Y.; Bolotin, K.; Zhao, Y.; Adam, S.; Hwang, E. H.; Das Sarma, S.; Stormer, H. L.; Kim, P. Measurement of scattering rate and minimum conductivity in graphene. *Phys. Rev. Lett.* **2007**, *99*, 24.

(21) Novoselov, K. S.; Geim, A. K.; Morozov, S. V.; Jiang, D.; Zhang, Y.; Dubonos, S. V.; Grigorieva, I. V.; Firsov, A. A. Electric field effect in atomically thin carbon films. *Science* **2004**, *306* (5696), 666−669.

(22) Zhang, Y. B.; Tan, Y. W.; Stormer, H. L.; Kim, P. Experimental observation of the quantum Hall effect and Berry's phase in graphene. *Nature* **2005**, *438* (7065), 201−204.

(23) Feldman, B. E.; Martin, J.; Yacoby, A. Broken-symmetry states and divergent resistance in suspended bilayer graphene. *Nat. Phys.* **2009**, *5* (12), 889−893.
(24) Wehling, T. O.; Yuan, S.; Lichtenstein, A. I.; Geim, A. K.; Katsnelson, M. I. Resonant Scattering by Realistic Impurities in Graphene. *Phys. Rev. Lett.* **2010**, *105*, 5.
(25) Rossi, E.; Adam, S.; Das Sarma, S. Effective medium theory for disordered two-dimensional graphene. *Phys. Rev. B* **2009**, *79*, 24.